Far East Journal of Applied Mathematics

Published Online: October 2013
Available online at http://pphmj.com/journals/fjam.htm
Volume 80, Number 1, 2013, Pages 41-66

SORET AND DUFOUR EFFECTS ON HYDROMAGNETIC FREE CONVECTION FLOW WITH HEAT AND MASS TRANSFER PAST A POROUS PLATE IN THE PRESENCE OF CHEMICAL REACTION AND THERMAL RADIATION

P. O. Olanrewaju, A. Adeniyan and Sanmi Felix Alao

Department of Mathematics
Covenant University
Ota, Ogun State, Nigeria
e-mail: oladapo_anu@yahoo.ie

Department of Mathematics
University of Lagos
Lagos, Nigeria

Department of Mathematical Sciences
Federal University of Technology
Akure, Ondo State, Nigeria

Abstract

Analysis is presented for the influence of chemical reaction, thermal radiation, thermal-diffusion, diffusion-thermo on hydromagnetic free convection with heat and mass transfer past a vertical plate with suction/injection. Similarity solutions are obtained using suitable transformations. The ordinary differential equations are then solved

Received: June 18, 2013; Accepted: July 12, 2013
2010 Mathematics Subject Classification: 65L10, 20B40, 76E25.
Keywords and phrases: Soret and Dufour, heat and mass transfer, chemical reaction, thermal radiation, MHD flow.

numerically by applying Nachtsheim-Swigert shooting iteration technique together with sixth order Runge-Kutta integration scheme. The numerical results for some special cases have been compared with those obtained by Alam et al. [11] and are found in very good agreement. For fluids of medium molecular weight (H_2, air), the profiles of the dimensionless velocity, temperature and concentration distributions are shown graphically for various values of suction parameter f_w, Dufour number *Df*, Soret number *Sr*, chemical reaction parameter γ, order of reactions *n*, radiation parameter *Ra* and magnetic strength parameter *M*. In addition, the skin-friction coefficient, the Nusselt number and Sherwood number are shown in tabular forms.

1. Introduction

Chemical reaction can be codified as either heterogeneous or homogeneous processes. This depends on whether they occur at an interface or as a single-phase volume reaction. A few representative fields of interest in which combined heat and mass transfer with chemical reaction effect play an important role are design of chemical processing equipment, formation and dispersion of fog, distribution of temperature and moisture over agricultural fields and groves of fruit trees, damage of crops due to freezing, food processing and cooling towers. Cooling towers are the cheapest way to cool large quantities of water. In particular, the study of heat and mass transfer with chemical reaction is of considerable importance in chemical and hydrometallurgical industries. For example, formation of smog is a first order homogeneous chemical reaction. In nature, the presence of pure air or water is impossible. Some foreign mass may be present either naturally or mixed with the air or water. The present trend in the field of chemical reaction analysis is to give a mathematical model for the system to predict the reactor performance. A large amount of research work has been reported in this field. In particular, the study of heat and mass transfer with chemical reaction is of considerable importance in chemical and hydrometallurgical industries. Effects of heat and mass transfer on nonlinear boundary layer flow have been discussed by many authors (see [1-5]).

Convective heat transfer in porous media has been a subject of great interest for the last few decades. The research activities in this field has been accelerated because of a broad range of applications in various disciplines, such as geophysical, thermal and insulating engineering, modelling of packed sphere beds, solar power collector, pollutant dispersion in aquifers, cooling of electronic systems, ventilation of rooms, crystal growth in liquids, chemical catalytic reactors, grain storage devices, petroleum reservoirs, ground hydrology, fiber and granular insulation, nuclear waste repositories, high-performance building insulation, post-accident heat removal from pebble-bed nuclear reactors, concepts of aerodynamic heat shielding with transpiration cooling (see [6-10]).

Also the effect of thermal radiation on flow and heat transfer processes is of major importance in the design of many advanced energy conversion systems operating at high temperature. Thermal radiation within such systems occurs because of the emission by the hot walls and working fluid. Alam et al. [11], examined the Dufour and Soret effects on steady free convection and mass transfer flow past a semi-infinite vertical porous plate in a porous medium. Similarly, Alam and Rahman [12], investigated the Dufour and Soret effects on mixed convection flow past a vertical porous flat plate with variable suction. Osalusi et al. [13], studied the thermal-diffusion and diffusion-thermo effects on combined heat and mass transfer of a steady MHD convective and slip flow due to a rotating disk with viscous dissipation and Ohmic heating. Afify [14], examined the similarity solution for MHD, thermal-diffusion and diffusion-thermo effects on free convective heat and mass transfer over a stretching surface considering suction or injection. Hayat et al. [15] investigated the heat and mass transfer for Soret and Dufour effect on mixed convection boundary layer flow over a stretching vertical surface in a porous medium filled with a viscoelastic fluid. Recently, Olanrewaju [16] examined the Dufour and Soret effects of a transient free convective flow with radiative heat transfer past a flat plate moving through a binary mixture. Similarly, Shateyi et al. [17] studied the effects of thermal radiation, Hall currents, Soret and Dufour effects on MHD flow by mixed convection over a vertical surface in porous media.

The present paper considers the effects of chemical reaction, thermal radiation, Soret, and Dufour on hydromagnetic free convection with heat and mass transfer past a vertical plate considering suction or injection. Hence, the purpose of this study is to extend Alam et al. [11], to study the more general problem which includes chemical reaction, thermal radiation, Soret, and Dufour effects on free convection with heat and mass transfer past a vertical plate in the presence of magnetic field considering suction or injection. To the best of the authors, such work has not been considered. The analysis of the results obtained in the present work shows that the flow field is appreciably influenced by the Dufour and Soret numbers, chemical reaction, thermal radiation parameters and suction on the wall. To reveal the tendency of the solutions, selected results for the velocity components, temperature, and concentration are graphically depicted. The rest of the paper is structured as follows. In Section 2, we formulate the problem: in Section 3, we give the method of solution. Our results are presented and discussed in Section 4, and in Section 5, we present some brief conclusions.

2. Mathematical Analysis

A two-dimensional steady free convection and mass transfer flow of a viscous incompressible fluid past a continuously moving semi-infinite vertical porous flat plate in a porous medium is considered. The flow is assumed to be in the *x*-direction which is taken along the plate in the upward direction and the *y*-axis is taken normal to it. Then under the usual Boussinesq's approximation, the governing equations relevant to the problem are:

Continuity equation

$$\frac{\partial u}{\partial x} + \frac{\partial v}{\partial y} = 0. \tag{1}$$

Momentum equation

$$u\frac{\partial u}{\partial x} + v\frac{\partial u}{\partial y} = \upsilon\frac{\partial^2 u}{\partial y^2} + g\beta(T - T_\infty) + g\beta^*(C - C_\infty) - \frac{\upsilon}{K'}u - \frac{\sigma_e B_0^2 u}{\rho}. \tag{2}$$

Energy equation

$$u\frac{\partial T}{\partial x}+v\frac{\partial T}{\partial y}=\alpha\frac{\partial^2 T}{\partial y^2}+\frac{D_m k_T}{c_s c_p}\frac{\partial^2 C}{\partial y^2}-\frac{\alpha}{k}\frac{\partial q_r}{\partial y}. \tag{3}$$

Concentration equation

$$u\frac{\partial C}{\partial x}+v\frac{\partial C}{\partial y}=D_m\frac{\partial^2 C}{\partial y^2}+\frac{D_m k_T}{T_m}\frac{\partial^2 T}{\partial y^2}-R^*(C-C_\infty)^n, \tag{4}$$

where u, v are the velocity components in the x and y directions, respectively, υ is the kinematic viscosity, g is the acceleration due to gravity, ρ is the density, β is the coefficient of volume expansion, β^* is the volumetric coefficient of expansion with concentration, T, T_w and T_∞ are the temperature of the fluid inside the thermal boundary layer, the plate temperature and the fluid temperature in the free stream, respectively, while C, C_w and C_∞ are the corresponding concentrations. Also, K' is the permeability of a porous medium, α is the thermal diffusivity, D_m is the coefficient of mass diffusivity, c_p is the specific heat at constant pressure, T_m is the mean fluid temperature, k_T is the thermal-diffusion ratio, and c_s is the concentration susceptibility, R^* is the rate of chemical reaction and n is the order of reaction.

The boundary conditions for the model are

$$\begin{aligned} &u=U_0,\ \ v=v_0(x),\ \ T=T_w,\ \ C=C_w \quad \text{at} \quad y=0,\\ &u=0,\ \ v=0,\ \ T=T_w,\ \ C=C_w \quad \text{as} \quad y\to\infty, \end{aligned} \tag{5}$$

where U_0 is the uniform velocity and $v_0(x)$ is the velocity of suction at the plate.

The radiative heat flux q_r is described by Roseland approximation such that

$$q_r=-\frac{4\sigma^*}{3K}\frac{\partial T^4}{\partial y}, \tag{6}$$

where σ^* and K are the Stefan-Boltzmann constant and the mean absorption coefficient, respectively. Following Shateyi et al. [17], we assume that the temperature differences within the flow are sufficiently small so that the T^4 can be expressed as a linear function after using Taylor series to expand T^4 about the free stream temperature T_∞ and neglecting higher-order terms. This result is the following approximation:

$$T^4 \approx 4T_\infty^3 T - 3T_\infty^4. \tag{7}$$

Using (6) and (7) in (3), we obtain

$$\frac{\partial q_r}{\partial y} = -\frac{16\sigma^*}{3K}\frac{\partial T^4}{\partial y}. \tag{8}$$

Following Alam et al. [11], we nondimensionalize (1)-(4) using the following transformations:

$$\eta = y\sqrt{\frac{U_0}{2\upsilon x}}, \quad \psi = \sqrt{\upsilon v U_0}\, f(\eta), \quad \theta(\eta) = \frac{T - T_\infty}{T_w - T_\infty}, \quad \phi(\eta) = \frac{C - C_\infty}{C_w - C_w}, \tag{9}$$

where $f(\eta)$ is the dimensionless stream function and ψ is the dimensionless stream function defined by $u = \frac{\partial \psi}{\partial x}$ and $v = -\frac{\partial \psi}{\partial y}$, just to satisfy the equation of continuity (1).

We then introduce the relation (6), into equation (1) and obtain

$$u = U_0 f'(\eta) \quad \text{and} \quad v = \sqrt{\frac{\upsilon U_0}{2x}}(\eta f' - f). \tag{10}$$

Substituting equations (6) and (7) into equations (2)-(4), we have

$$f''' + ff'' + Gr\theta + Gm\phi - Kf' - Mf' = 0, \tag{11}$$

$$\theta''\left(1 + \frac{4}{3}R_d\right) + Prf\theta' + PrDf\phi'' = 0, \tag{12}$$

$$\phi'' + Scf\phi' + ScSr\theta'' - Sc\gamma\phi^n = 0, \tag{13}$$

where

$Gr = \dfrac{g\beta(T_w - T_\infty)2x}{U_0^2}$ is the Grashof number,

$Gm = \dfrac{g\beta^*(C_w - C_\infty)2x^2}{\upsilon U_0}$ is the modified Grashof number,

$K = \dfrac{2\upsilon x}{K'U_0}$ is the permeability parameter,

$Pr = \dfrac{\upsilon}{\alpha}$ is the Prandtl number,

$Sc = \dfrac{\upsilon}{D_m}$ is the Schmidt number,

$Sr = \dfrac{D_m k_T(T_w - T_\infty)}{\upsilon T_m(C_w - C_\infty)}$ is the Soret number,

$Df = \dfrac{D_m k_T(C_w - C_\infty)}{c_s c_p \upsilon(T_w - T_\infty)}$ is the Dufour number,

$R_d = \dfrac{4\sigma^* T_\infty^3}{k\alpha}$ is the radiation parameter,

$M = \dfrac{2\sigma^* B_0^2 x}{\rho U_0}$ is magnetic strength parameter and

$\gamma = 2R^* x(C_w - C_\infty^{/})^{n-1}$ is the chemical reaction parameter.

The corresponding boundary conditions are

$$f = f_w, \quad f' = 1, \quad \theta = 1, \quad \phi = 1 \quad \text{at} \quad \eta = 0,$$

$$f' = 0, \quad \theta = 0, \quad \phi = 0 \quad \text{as} \quad \eta \to \infty, \tag{14}$$

where $f_w = -v_0\sqrt{\dfrac{2x}{\upsilon U_0}}$ the dimensionless suction velocity and primes denote partial differentiation with respect to the variable η.

The parameters of engineering interest for the present problem are the local skin-friction coefficient, the local Nusselt number and the local Sherwood number, which are given, respectively, by the following expressions:

$$\frac{1}{2}\,\mathrm{Re}^{1/2}\,C_f = f''(0), \tag{15}$$

$$Nu(\mathrm{Re})^{-1/2} = -\theta'(0), \tag{16}$$

$$Sh(\mathrm{Re})^{-1/2} = -\phi'(0), \tag{17}$$

where $\mathrm{Re} = \dfrac{U_0 x}{\upsilon}$ is the Reynold's number.

3. Computational Procedure

The set of equations (11)-(13) together with the boundary conditions (14) have been solved numerically by applying Nachtsheim-Swigert shooting iteration technique along with Runge-Kutta sixth order integration method. From the process of numerical computation, the skin-friction coefficient, the local Nusselt number and the local Sherwood number, which are, respectively, proportional to $f''(0)$, $-\theta'(0)$ and $-\phi'(0)$, are also sorted out and their numerical values are presented in a tabular form. The computations have been performed by a program which uses a symbolic and computational computer language MAPLE [18]. A step size of $\Delta\eta = 0.001$ is selected to be satisfactory for a convergence criterion of 10^{-7} in nearly all cases. The value of y_∞ is found to each iteration loop by the assignment statement $\eta_\infty = \eta_\infty + \Delta\eta$. The maximum value of η_∞, to each group of parameters, *Pr*, *Sc*, *Sr*, *Df*, *M*, *Ra*, *Gr*, *K*, *Gm*, γ, *M* and f_w is determined when the values of unknown boundary conditions at $\eta = 0$ do not change to successful loop with error less than 10^{-7}.

4. Results and Discussions

In order to get a clear insight of the physical problem, the velocity, temperature and concentration have been discussed by assigning numerical values to the parameters encountered in the problem. To be realistic, the values of Schmidt number (*Sc*) are chosen for hydrogen $(Sc = 0.22)$, water vapour $(Sc = 0.62)$, ammonia $(Sc = 0.78)$ and Propyl Benzene $(Sc = 2.62)$ at temperature 25°C and one atmospheric pressure. The values of Prandtl number is chosen to be $Pr = 0.71$ which represents air at temperature 25°C and one atmospheric pressure. Attention is focused on positive values of the buoyancy parameters, i.e., Grashof number $G_r > 0$ (which corresponds to the cooling problem) and solutal Grashof number $G_m > 0$ (which indicates that the chemical species concentration in the free stream region is less than the concentration at the boundary surface). In Table 1, comparison is made for some fixed parameters and there is a perfect agreement with Alam et al. [11] which is a special case of ours. We went further in Table 2 to generate the skin-friction coefficient, Nusselt number and the Sherwood number for some embedded parameters value in the flow model. Here, the values of Dufour number and Soret number are chosen so that their product is constant provided that the mean temperature is also kept constant. It is clearly seen that an increase in the parameters M, f_w, Pr, Ra and γ leads to an increase in the skin-friction at the wall of the plate while increase in parameters *Gr*, *Gm*, *Sc*, *Df*, *Sr*, *K* and *n* decreases the skin-friction at the wall surface. Similarly, the Nusselt number coefficient increases at the wall plate when *Gr*, *Sc*, *Pr*, *Ra* and γ increases while it decreases at the wall plate when parameters *M*, *Df*, *Sr*, *K* and *n* increases. It is also observed that injection increases the fluid flow while suction reduces the fluid flow velocity.

Table 1. Computations showing comparison of C_f, Nu and Sh number with Alam et al. [11] for $Gr = 10$, $Gm = 4$, $f_w = 0.5$, $K = 0.3$, $Pr = 0.71$, $Sc = 0.22$, $M = 0$, $n = 0$ and $\gamma = 0$

		Present	Present	Present	Alam et al. [11]	Alam et al. [11]	Alam et al. [11]
Df	*Sr*	*Cf*	*Nu*	*Sh*	C_f	*Nu*	*Sh*
0.030	2.0	6.22854	1.15657	0.15312	6.2285	1.1565	0.1531
0.037	1.6	6.14913	1.15013	0.22834	6.1491	1.1501	0.2283
0.050	1.2	6.07209	1.14282	0.30336	6.0720	1.1428	0.3033
0.075	0.8	6.00067	1.13333	0.37819	6.0006	1.1333	0.3781
0.150	0.4	5.95538	1.11573	0.45400	5.9553	1.1157	0.4540

Table 2. Computations showing $-f''(0)$, $-\theta'(0)$ and $-\phi'(0)$ for various embedded parameters

M	*Gr*	*Gm*	f_w	*Sc*	*Pr*	*Df*	*Sr*	*Ra*	*K*	*Γ*	*n*	$-f''(0)$	$-\theta'(0)$	$-\phi'(0)$
0.1	0.5	0.2	0.1	0.22	0.71	0.030	2	1	0.2	1	1	0.46637	1.58917	0.04166
0.4	0.5	0.2	0.1	0.22	0.71	0.030	2	1	0.2	1	1	0.63593	1.59963	0.02827
0.6	0.5	0.2	0.1	0.22	0.71	0.035	2	1	0.2	1	1	0.73874	1.60466	0.02085
0.1	4.0	0.2	0.1	0.22	0.71	0.030	2	1	0.2	1	1	-0.2653	1.62226	0.01348
0.1	10.0	0.2	0.1	0.22	0.71	0.030	2	1	0.2	1	1	-1.4706	1.62831	0.01224
0.1	0.5	2.0	0.1	0.22	0.71	0.030	2	1	0.2	1	1	-1.1444	1.29951	0.26796
0.1	0.5	5.0	0.1	0.22	0.71	0.030	2	1	0.2	1	1	-3.3281	0.96406	0.50802
0.1	0.5	10.0	0.1	0.22	0.71	0.030	2	1	0.2	1	1	-6.4245	0.56447	0.78611
0.1	0.5	0.2	0.5	0.22	0.71	0.030	2	1	0.2	1	1	0.70365	1.86320	-0.0480
0.1	0.5	0.2	1.0	0.22	0.71	0.030	2	1	0.2	1	1	1.05104	2.20659	-0.1552
0.1	0.5	0.2	-0.5	0.22	0.71	0.030	2	1	0.2	1	1	0.18567	1.18822	0.17657
0.1	0.5	0.2	0.1	0.62	0.71	0.030	2	1	0.2	1	1	0.47899	1.60390	-0.2324
0.1	0.5	0.2	0.1	0.78	0.71	0.030	2	1	0.2	1	1	0.47964	1.60722	-0.3398
0.1	0.5	0.2	0.1	2.62	0.71	0.030	2	1	0.2	1	1	0.47336	1.63260	-1.3981
0.1	0.5	0.2	0.1	3.00	0.71	0.030	2	1	0.2	1	1	0.47186	1.63683	-1.5914
0.1	0.5	0.2	0.1	0.22	3.0	0.030	2	1	0.2	1	1	0.44592	2.21993	-0.2244
0.1	0.5	0.2	0.1	0.22	7.1	0.030	2	1	0.2	1	1	0.45204	3.21900	-0.6556
0.1	0.5	0.2	0.1	0.22	10	0.030	2	1	0.2	1	1	0.45704	3.89509	-0.9496
0.1	0.5	0.2	0.1	0.22	0.71	0.050	2	1	0.2	1	1	0.46494	1.58877	0.04178
0.1	0.5	0.2	0.1	0.22	0.71	0.150	2	1	0.2	1	1	0.45790	1.58701	0.04226
0.1	0.5	0.2	0.1	0.22	0.71	0.030	4	1	0.2	1	1	0.41851	1.58765	-0.4553
0.1	0.5	0.2	0.1	0.22	0.71	0.030	8	1	0.2	1	1	0.32111	1.58137	-1.4224
0.1	0.5	0.2	0.1	0.22	0.71	0.035	2	2	0.2	1	1	0.68739	2.77423	-0.4383
0.1	0.5	0.2	0.1	0.22	0.71	0.030	2	3	0.2	1	1	0.86506	4.05192	-0.9671
0.1	0.5	0.2	0.1	0.22	0.71	0.030	2	1	0.4	1	1	0.46637	1.58917	0.04166
0.1	0.5	0.2	0.1	0.22	0.71	0.030	2	1	0.8	1	1	0.46637	1.58917	0.04166
0.1	0.5	0.2	0.1	0.22	0.71	0.030	2	1	0.2	2	1	0.49761	1.59377	0.27602
0.1	0.5	0.2	0.1	0.22	0.71	0.030	2	1	0.2	3	1	0.51567	1.59438	0.45566
0.1	0.5	0.2	0.1	0.22	0.71	0.030	2	1	0.2	1	3	0.42925	1.57210	-0.0396
0.1	0.5	0.2	0.1	0.22	0.71	0.030	2	1	0.2	1	5	0.41869	1.56730	-0.0620

A. Velocity profiles

Figures 1-7 depict the solutions of velocity across the boundary layer for the embedded parameters in the flow model against spanwise coordinate η. In Figure 1, we display the solution of velocity profile across the boundary layer for different values of the magnetic strength parameter *M* and it is observed that increasing the magnetic strength parameter value decreases the velocity of the fluid flow which stabilizes the flow. Figure 2 depicts the plot of velocity against η for various values of the thermal Grashof number. It is clearly seen from the figure that increases in the thermal Grashof number increases the velocity boundary layer thickness. It is interesting to note that when $Gr \geq 2$, there was a sudden increase in the velocity boundary layer thickness close to the wall plate before coming down to satisfy the boundary condition far away to the plate. In Figure 3, it can be seen that the same effect occurs as in Figure 2. Increasing the solutal Grashof number decreases the velocity boundary layer thickness as expected. The effect of suction/ injection is displayed in Figure 4 and it is established that suction decreases the velocity boundary layer thickness while injection increases the velocity boundary layer thickness. It is quite interesting to note that suction stabilizes fluid flow. It is noteworthy to mention that radiation parameter and chemical reaction parameter reduce the velocity boundary layer thickness in Figures 5 and 6 while increasing the order of reaction increases the velocity boundary layer thickness slightly (as can be seen in Figure 7).

B. Temperature profiles

Figures 8-14, depict the solutions of temperature across the boundary layer for the embedded flow parameters controlling the model against the spanwise coordinate η. Increasing the magnetic strength parameter increases the thermal boundary layer (see Figure 8). In Figures 9 and 10, we observed that increasing the thermal Grashof and the solutal Grashof number decreases the thermal boundary layer thickness. It is quite interesting to note that when

$Gm = 2$, there is a reversed flow. In Figure 11, the suction parameter decreases the thermal boundary layer thickness while injection increases the thermal boundary layer thickness across the layer boundary. Figure 12 depicts the solution of temperature against η for various values of Prandtl numbers *Pr* and it is observed that increasing *Pr* decreases the thermal boundary layer thickness while increasing Dufour number *Df* increases the thermal boundary layer thickness (see Figure 13). Finally, Figure 14 shows the influence of radiation parameter *Ra* on the thermal boundary layer thickness. Increasing the radiation parameter *Ra* leads to a decrease in the thermal boundary layer thickness. It is noteworthy that there are reversed flows.

C. Concentration profiles

Figures 15-23 shows the solutions of the concentration across the boundary layer for various embedded parameters controlling the flow model. In Figure 15, we observed that an increase in the thermal Grashof number *Gr* decreases the concentration boundary layer thickness. Similar effect is noticed in Figure 16. In Figure 17, we found that suction reduces the concentration boundary layer while injection thickens the concentration boundary layer. The effect of Schmidt number *Sc* on the concentration profile is presented in Figure 18. Increasing *Sc* is to decrease the concentration boundary layer thickness. The influence of Prandtl number, Soret number and the radiation parameter are shown in Figures 19-21. Increase in these parameters lead to an increase in the concentration boundary layer thickness. It is interesting to note that the concentration is at the peak close to the wall plate when Soret number increases. In Figure 22, it is seen that the concentration of the fluid decreases with an increase in destructive reaction $(\gamma > 0)$ of the chemical reaction whereas the velocity and temperature of the fluid significant increase for destructive reaction. The concentration boundary layer thickness increases in Figure 23 when the order of chemical reaction *n* increases.

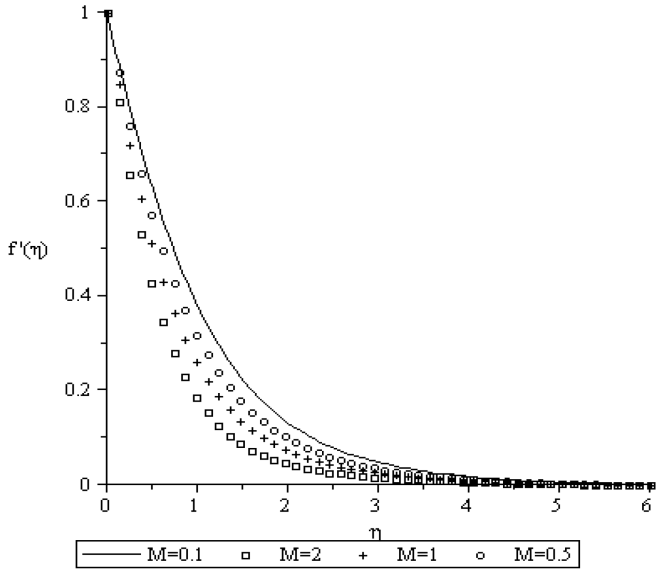

Figure 1. Velocity profiles for $Gr = 0.1$, $Gm = 0.1$, $f_w = 0.5$, $Sc = 0.22$, $Pr = 0.71$, $Df = 0.03$, $Sr = 2$, $Ra = \gamma = n = 1$, $K = 0.2$.

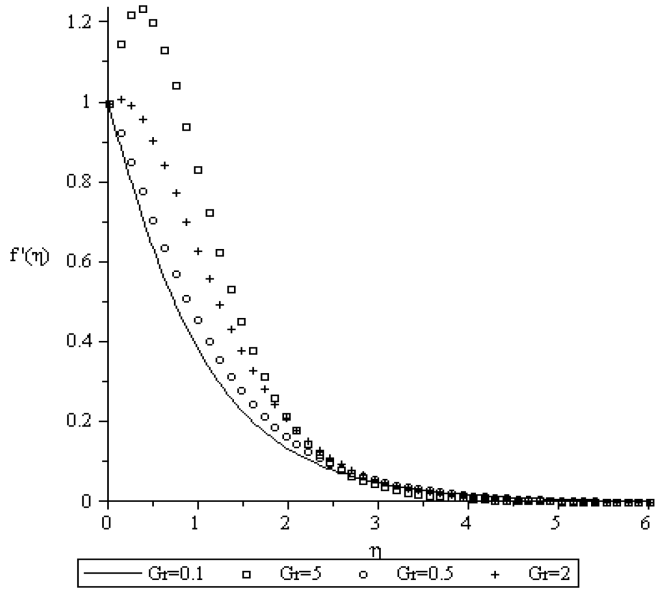

Figure 2. Velocity profiles for $M = 0.1$, $Gm = 0.1$, $f_w = 0.5$, $Sc = 0.22$, $Pr = 0.71$, $Df = 0.03$, $Sr = 2$, $Ra = \gamma = n = 1$, $K = 0.2$.

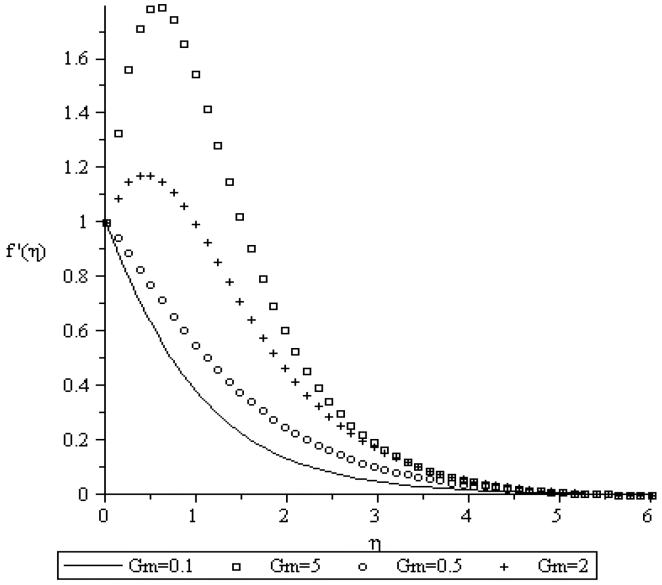

Figure 3. Velocity profiles for $M = 0.1$, $Gr = 0.1$, $f_w = 0.5$, $Sc = 0.22$, $Pr = 0.71$, $Df = 0.03$, $Sr = 2$, $Ra = \gamma = n = 1$, $K = 0.2$.

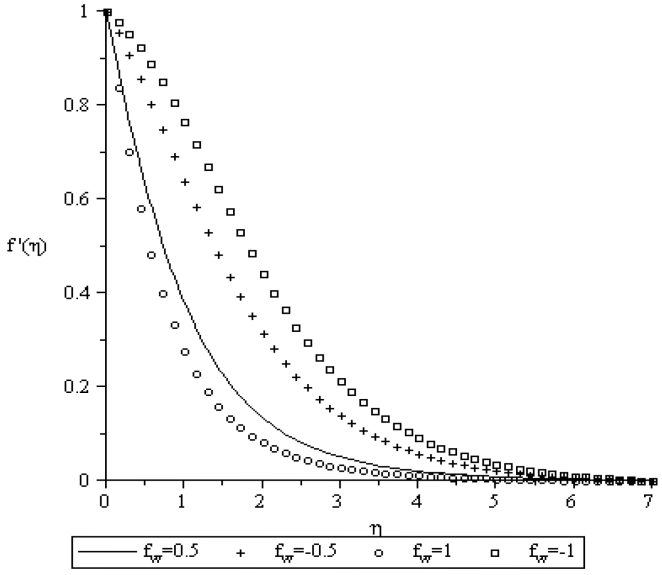

Figure 4. Velocity profiles for $M = 0.1$, $Gr = 0.1$, $Gm = 0.1$, $Sc = 0.22$, $Pr = 0.71$, $Df = 0.03$, $Sr = 2$, $Ra = \gamma = n = 1$, $K = 0.2$.

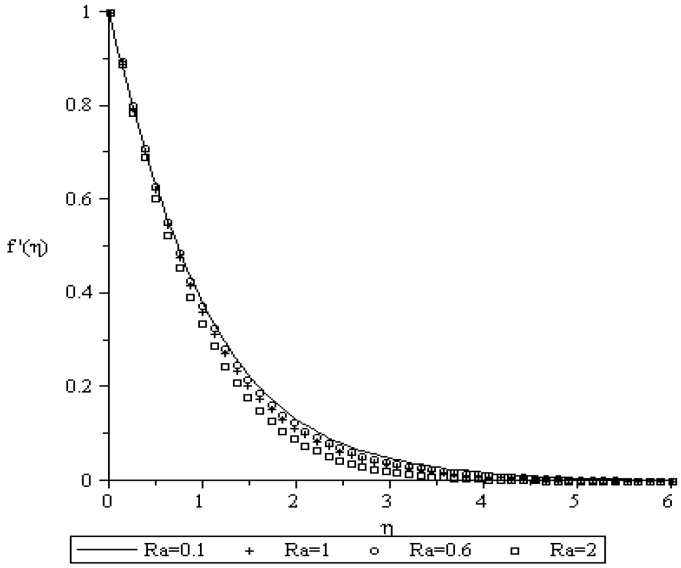

Figure 5. Velocity profiles for $M = 0.1$, $Gr = 0.1$, $Gm = 0.1$, $f_w = 0.5$, $Pr = 0.71$, $Df = 0.03$, $\gamma = n = 1$, $K = 0.2$, $Sc = 0.22$, $Sr = 2$.

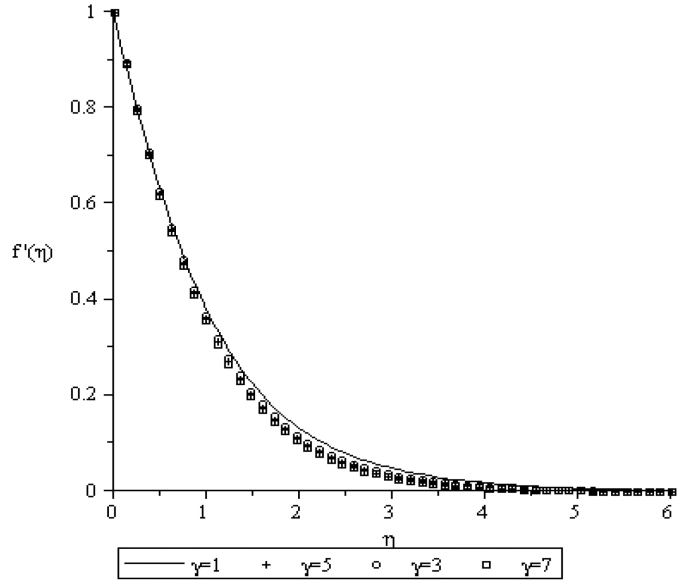

Figure 6. Velocity profiles for $M = 0.1$, $Gr = 0.1$, $Gm = 0.1$, $f_w = 0.5$, $Pr = 0.71$, $Df = 0.03$, $n = 1$, $K = 0.2$, $Sc = 0.22$, $Sr = 2$, $Ra = 1$.

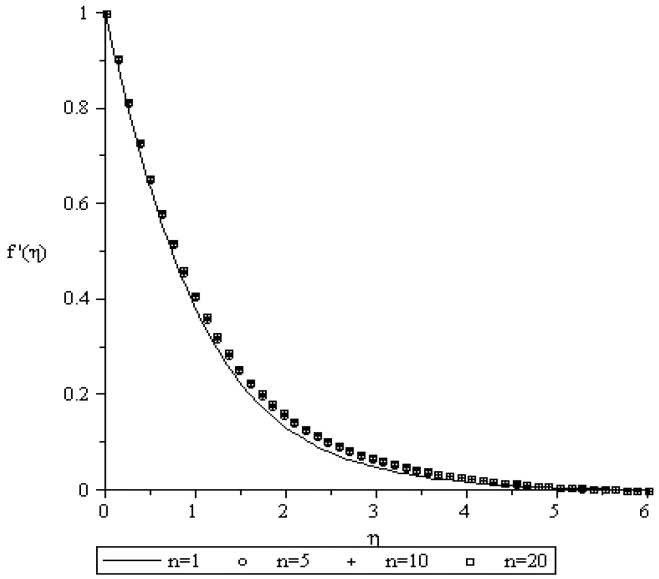

Figure 7. Velocity profiles for $M = 0.1$, $Gr = 0.1$, $Gm = 0.1$, $f_w = 0.5$, $Pr = 0.71$, $Df = 0.03$, $K = 0.2$, $Sc = 0.22$, $Sr = 2$, $Ra = \gamma = 1$.

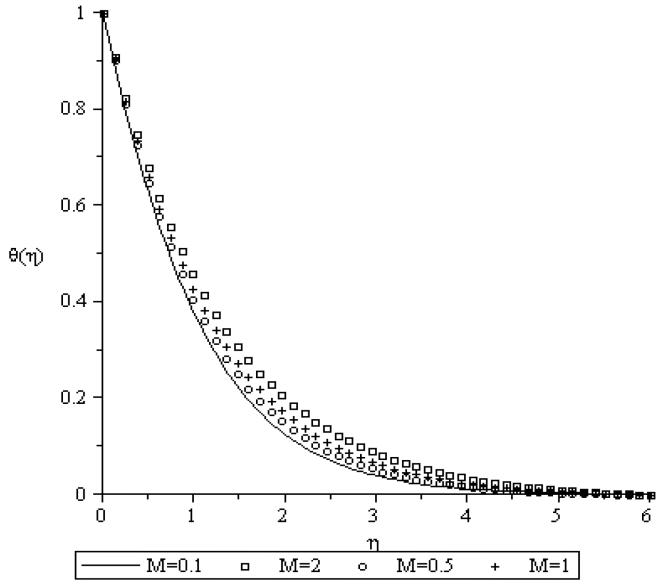

Figure 8. Temperature profiles for $Gr = 0.1$, $Gm = 0.1$, $f_w = 0.5$, $Sc = 0.22$, $Pr = 0.71$, $Df = 0.03$, $Sr = 2$, $Ra = \gamma = n = 1$, $K = 0.2$.

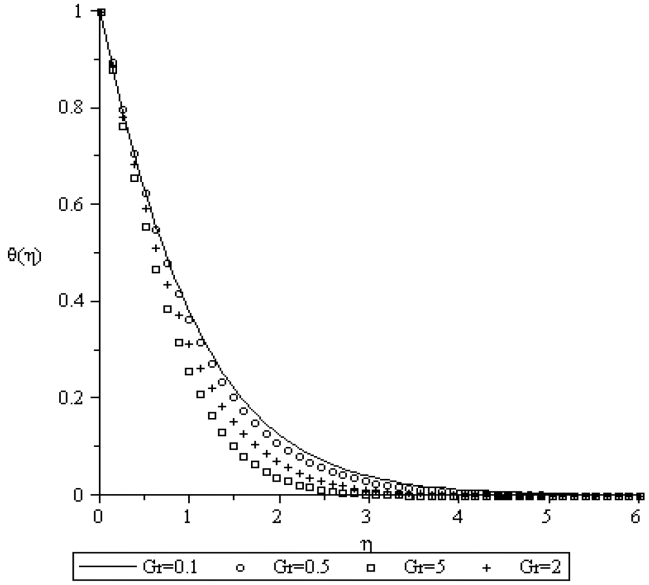

Figure 9. Temperature profiles for $M = 0.1$, $Gm = 0.1$, $f_w = 0.5$, $Sc = 0.22$, $Pr = 0.71$, $Df = 0.03$, $Sr = 2$, $Ra = \gamma = n = 1$, $K = 0.2$.

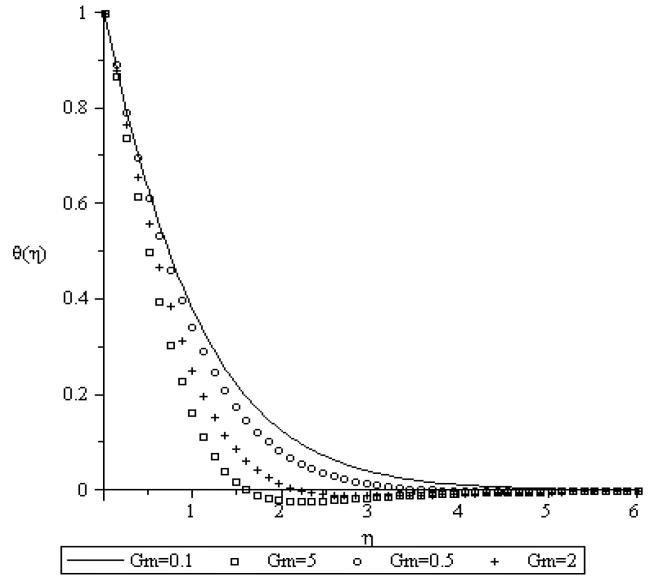

Figure 10. Temperature profiles for $M = 0.1$, $Gr = 0.1$, $f_w = 0.5$, $Sc = 0.22$, $Pr = 0.71$, $Df = 0.03$, $Sr = 2$, $Ra = \gamma = n = 1$, $K = 0.2$.

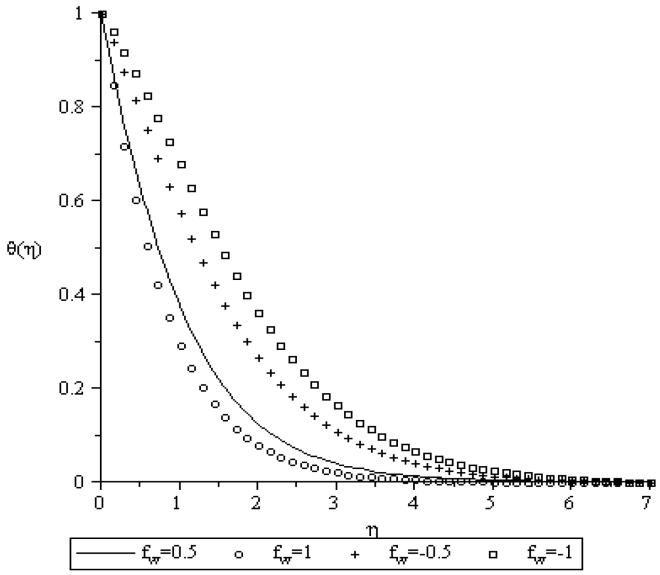

Figure 11. Temperature profiles for $M = 0.1$, $Gr = 0.1$, $Gm = 0.1$, $Sc = 0.22$, $Pr = 0.71$, $Df = 0.03$, $Sr = 2$, $Ra = \gamma = n = 1$, $K = 0.2$.

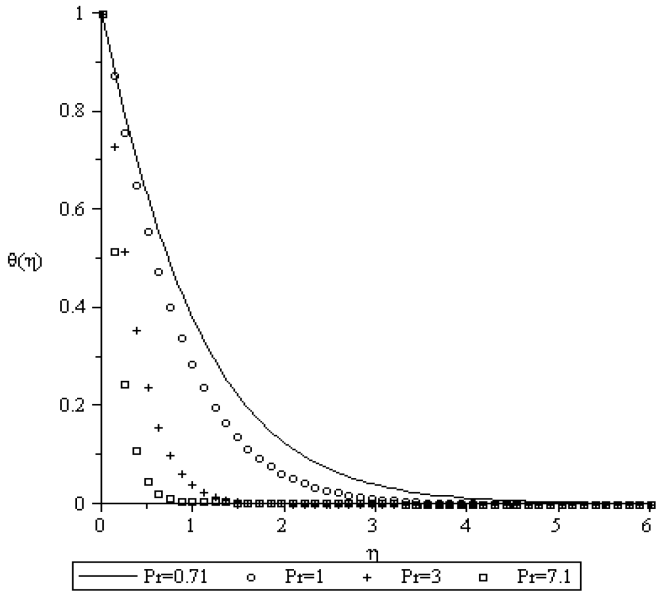

Figure 12. Temperature profiles for $M = 0.1$, $Gr = 0.1$, $Gm = 0.1$, $f_w = 0.5$, $Df = 0.03$, $Sr = 2$, $Ra = \gamma = n = 1$, $K = 0.2$, $Sc = 0.22$.

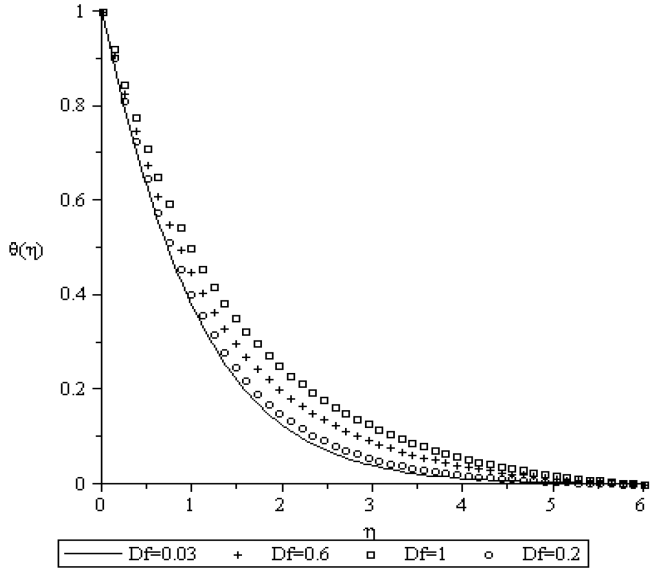

Figure 13. Temperature profiles for $M = 0.1$, $Gr = 0.1$, $Gm = 0.1$, $f_w = 0.5$, $Pr = 0.71$, $Sr = 2$, $Ra = \gamma = n = 1$, $K = 0.2$, $Sc = 0.22$.

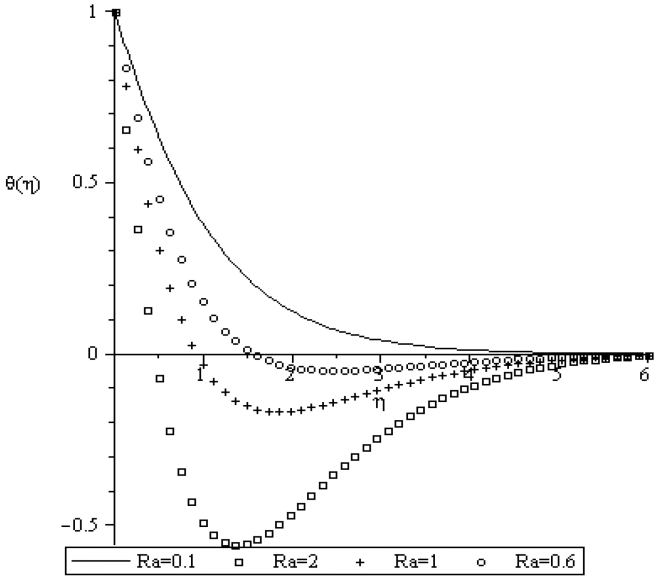

Figure 14. Temperature profiles for $M = 0.1$, $Gr = 0.1$, $Gm = 0.1$, $f_w = 0.5$, $Pr = 0.71$, $Df = 0.03$, $\gamma = n = 1$, $K = 0.2$, $Sc = 0.22$, $Sr = 2$.

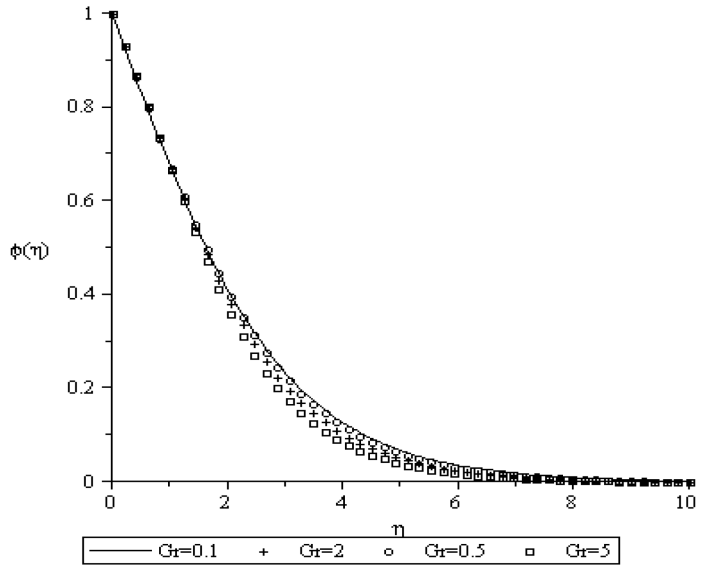

Figure 15. Concentration profiles for $M = 0.1$, $Gm = 0.1$, $f_w = 0.5$, $Sc = 0.22$, $Pr = 0.71$, $Df = 0.03$, $Sr = 2$, $Ra = \gamma = n = 1$, $K = 0.2$.

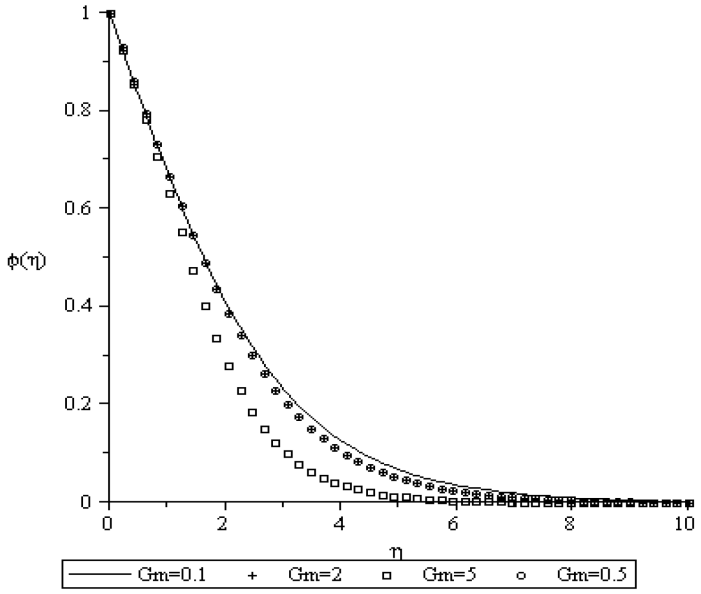

Figure 16. Concentration profiles for $M = 0.1$, $Gr = 0.1$, $f_w = 0.5$, $Sc = 0.22$, $Pr = 0.71$, $Df = 0.03$, $Sr = 2$, $Ra = \gamma = n = 1$, $K = 0.2$.

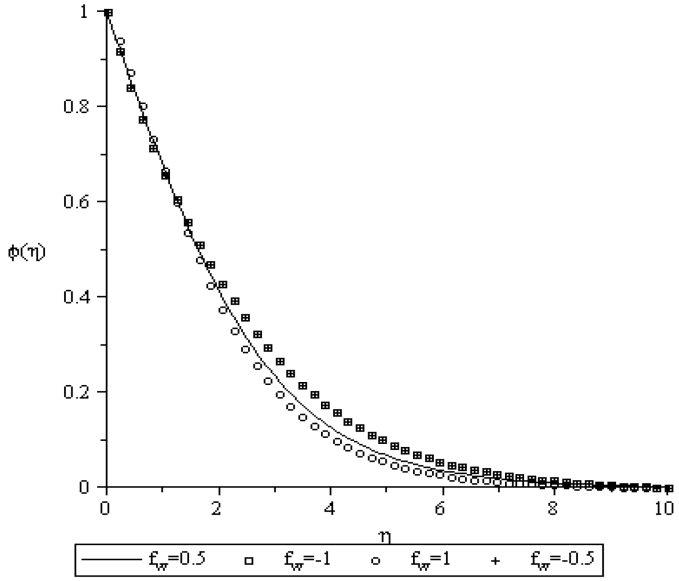

Figure 17. Concentration profiles for $M = 0.1$, $Gr = 0.1$, $Gm = 0.1$, $Sc = 0.22$, $Pr = 0.71$, $Df = 0.03$, $Sr = 2$, $Ra = \gamma = n = 1$, $K = 0.2$.

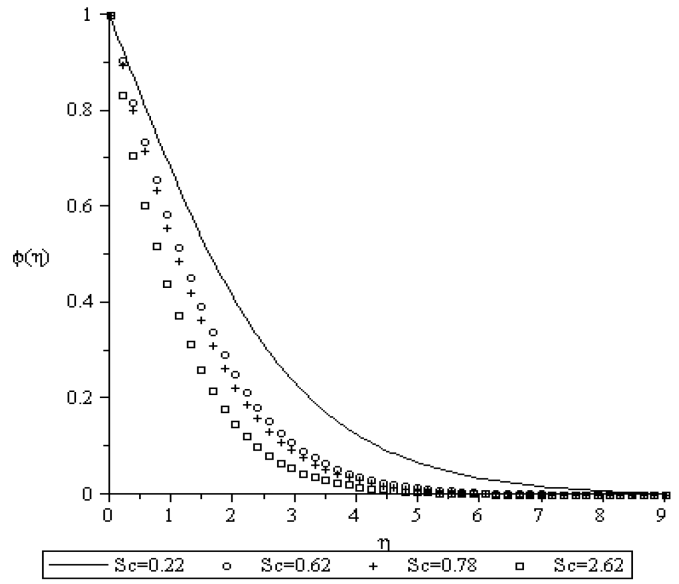

Figure 18. Concentration profiles for $M = 0.1$, $Gr = 0.1$, $Gm = 0.1$, $f_w = 0.5$, $Pr = 0.71$, $Df = 0.03$, $Sr = 2$, $Ra = \gamma = n = 1$, $K = 0.2$.

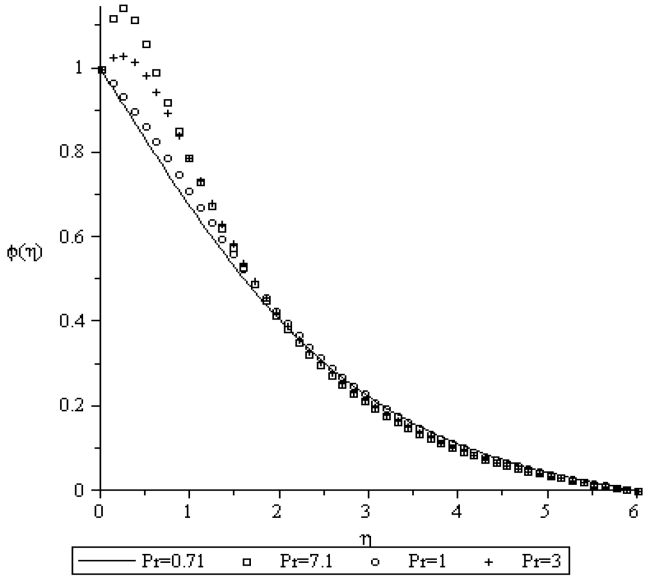

Figure 19. Concentration profiles for $M = 0.1,\ Gr = 0.1,\ Gm = 0.1,\ f_w = 0.5,\ Df = 0.03,\ Sr = 2,\ Ra = \gamma = n = 1,\ K = 0.2,\ Sc = 0.22.$

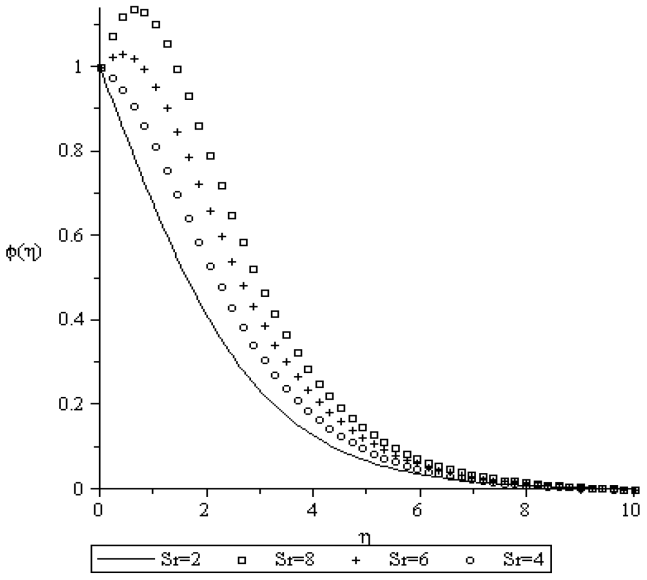

Figure 20. Concentration profiles for $M = 0.1,\ Gr = 0.1,\ Gm = 0.1,\ f_w = 0.5,\ Pr = 0.71,\ Df = 0.03,\ Ra = \gamma = n = 1,\ K = 0.2,\ Sc = 0.22.$

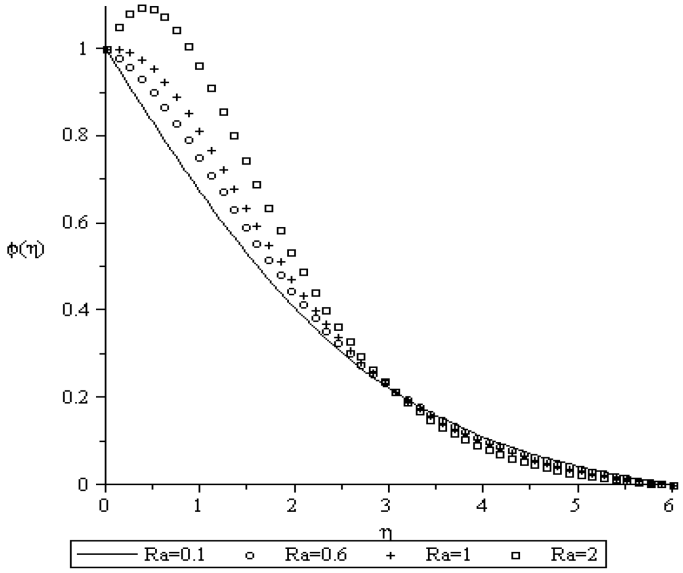

Figure 21. Concentration profile for $M = 0.1$, $Gr = 0.1$, $Gm = 0.1$, $f_w = 0.5$, $Pr = 0.71$, $Df = 0.03$, $\gamma = n = 1$, $K = 0.2$, $Sc = 0.22$, $Sr = 2$.

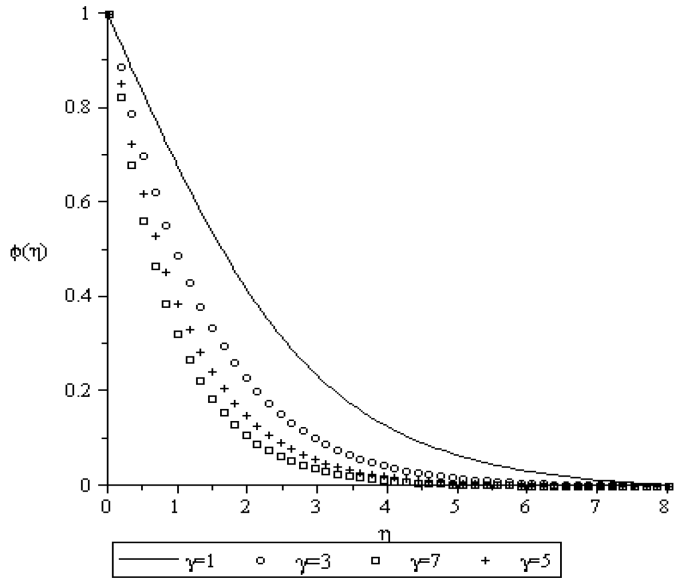

Figure 22. Concentration profiles for $M = 0.1$, $Gr = 0.1$, $Gm = 0.1$, $f_w = 0.5$, $Pr = 0.71$, $Df = 0.03$, $n = 1$, $K = 0.2$, $Sc = 0.22$, $Sr = 2$, $Ra = 1$.

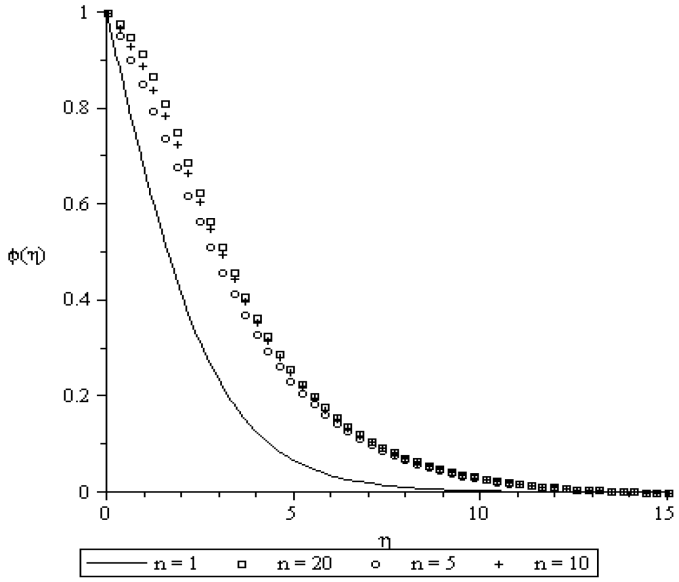

Figure 23. Concentration profiles for $M = 0.1$, $Gr = 0.1$, $Gm = 0.1$, $f_w = 0.5$, $Pr = 0.71$, $Df = 0.03$, $K = 0.2$, $Sc = 0.22$, $Sr = 2$, $Ra = \gamma = 1$.

5. Conclusions

In this work, the problem of the effects of chemical reaction, thermal radiation, Soret, and Dufour on hydromagnetic free convection with heat and mass transfer past a vertical plate considering suction or injection is investigated. The governing equations are transformed into nonlinear ordinary differential equations using similarity transformations, and then solved numerically by shooting technique with sixth order Runge-Kutta method. A parametric study is performed to explore the effects of various governing parameters on the fluid flow and heat and mass transfer characteristics. It is quite interesting to note that the order of reaction *n* and the chemical reaction parameter γ has opposite effects on the concentration boundary layer thickness. It is clearly seen that increase in the parameters *M*, f_w, *Pr*, *Ra* and γ leads to an increase in the skin-friction at the wall of the plate while increase in parameters *Gr*, *Gm*, *Sc*, *Df*, *Sr*, *K* and *n* decreases the

skin-friction at the wall surface. Similarly, the Nusselt number coefficient increases at the wall plate when *Gr*, *Sc*, *Pr*, *Ra* and γ increase while it decreases at the wall plate when parameters *M*, *Df*, *Sr*, *K* and *n* increase. It is also observed that injection increases the fluid flow while suction reduces the fluid flow velocity.

Acknowledgement

Dr. Olanrewaju would like to thank the financial support of Covenant University, Ota, Ogun State, Nigeria.

References

[1] S. N. Bhattacharyya and A. S. Gupta, On the stability of viscous flow over a stretching sheet, Quart. Appl. Math. 43 (1985), 359-367.

[2] J. F. Brady and A. Acrivo, Steady flow in a channel or tube with accelerating surface velocity, an exact solution to the Navier-Stokes equations with reverse flow, J. Fluid Mech. 112 (1981), 127-150.

[3] L. J. Crane, Flow past a stretching plate, ZAMP 21 (1970), 645-647.

[4] P. S. Gupta and A. S. Gupta, Heat and mass transfer on a stretching sheet with suction and blowing, Can. J. Chem. Eng. 55 (1977), 744-746.

[5] K. F. Jensen, E. O. Einset and D. I. Fotiadis, Flow phenomena in chemical vapour deposition of thin films, Annu. Rev. Fluid Mech. 23 (1991), 197-232.

[6] D. A. Nield and A. Bejan, Convection in Porous Media, 3rd ed., Springer, New York, 2006.

[7] D. B. Ingham and I. Pop, Transport Phenomena in Porous Media, Vol. 111, Elsevier, Oxford, 2005.

[8] I. Pop and D. B. Ingham, Convective Heat Transfer: Mathematical and Computational Modelling of Viscous Fluid and Porous Media, Pergamon, Oxford, 2001.

[9] A. Bejan, I. Dincer, S. Lorente, A. F. Miguel and A. H. Reis, Porous and Complex Flow Structures in Modern Technology, Springer, New York, 2004.

[10] K. Vafai, Ed., Handbook of Porous Media, Marcel Dekker, New York, 2000.

[11] M. S. Alam, M. Ferdows, M. Ota and M. A. Maleque, Dufour and Soret effects on steady free convection and mass transfer flow past a semi-infinite vertical porous plate in a porous medium, Int. J. of Applied Mechanics and Engineering 11(3) (2006), 535-545.

[12] M. S. Alam and M. M. Rahman, Dufour and Soret effects on mixed convection flow past a vertical porous flat plate with variable suction, Nonlinear Anal. Model. Control 11(1) (2006), 3-12.

[13] E. Osalusi, J. Side and R. Harris, Thermal-diffusion and diffusion-thermo effects on combined heat and mass transfer of a steady MHD convective and slip flow due to a rotating disk with viscous dissipation and Ohmic heating, International Communications in Heat and Mass Transfer 35 (2009), 908-915.

[14] A. A. Afify, Similarity solution in MHD: effects of thermal diffusion and diffusion thermo on free convective heat and mass transfer over a stretching surface considering suction or injection, Commun. Nonlinear Sci. Numer. Simul. 14(5) (2009), 2202-2214.

[15] T. Hayat, M. Mustafa and I. Pop, Heat and mass transfer for Soret and Dufour's effect on mixed convection boundary layer flow over a stretching vertical surface in a porous medium filled with a viscoelastic fluid, Commun. Nonlinear Sci. Numer. Simul. 15 (2010), 1183-1196.

[16] P. O. Olanrewaju, Dufour and Soret effects of a transient free convective flow with radiative heat transfer past a flat moving through a binary mixture, Pacific Journal of Science and Technology 11(1) (2010), 163-172.

[17] S. Shateyi, S. S. Motsa and P. Sibanda, The effects of thermal radiation, Hall currents, Soret, and Dufour on MHD flow by mixed convection over a vertical surface in porous media, Math. Probl. Eng. 2010 (2010), 1-20.

[18] A. Heck, Introduction to Maple, 3rd ed., Springer-Verlag, 2003.